
Score-based Generative Modeling of Graphs via the System of Stochastic Differential Equations

Jaehyeong Jo^{1*} Seul Lee^{1*} Sung Ju Hwang^{1,2}

Abstract

Generating graph-structured data requires learning the underlying distribution of graphs. Yet, this is a challenging problem, and the previous graph generative methods either fail to capture the permutation-invariance property of graphs or cannot sufficiently model the complex dependency between nodes and edges, which is crucial for generating real-world graphs such as molecules. To overcome such limitations, we propose a novel score-based generative model for graphs with a continuous-time framework. Specifically, we propose a new graph diffusion process that models the joint distribution of the nodes and edges through a system of stochastic differential equations (SDEs). Then, we derive novel score matching objectives tailored for the proposed diffusion process to estimate the gradient of the joint log-density with respect to each component, and introduce a new solver for the system of SDEs to efficiently sample from the reverse diffusion process. We validate our graph generation method on diverse datasets, on which it either achieves significantly superior or competitive performance to the baselines. Further analysis shows that our method is able to generate molecules that lie close to the training distribution yet do not violate the chemical valency rule, demonstrating the effectiveness of the system of SDEs in modeling the node-edge relationships.

1. Introduction

Learning the underlying distribution of graph-structured data is an important yet challenging problem that has

^{*}Equal contribution ¹Korea Advanced Institute of Science and Technology (KAIST), Seoul, South Korea ²AITRICS, South Korea. Correspondence to: Jaehyeong Jo <harryjo97@kaist.ac.kr>, Seul Lee <ellenlee7890@gmail.com>, Sung Ju Hwang <sjhwang82@kaist.ac.kr>.

Preliminary work. Under review by the International Conference on Machine Learning (ICML). Do not distribute.

wide application, such as understanding the social networks (Grover et al., 2019; Wang et al., 2018), drug design (Simonovsky & Komodakis, 2018; Li et al., 2018c), neural architecture search (NAS) (Xie et al., 2019; Lee et al., 2021), and even program synthesis (Brockschmidt et al., 2019). Recently, deep generative models have shown success on graph generation by modeling complicated structural properties of graphs, exploiting the expressivity of neural networks. Among them, autoregressive models (You et al., 2018b; Liao et al., 2019) construct a graph via sequential decisions, while one-shot generative models (De Cao & Kipf, 2018; Liu et al., 2019) generate components of a graph at once. Although these models have achieved a certain degree of success, they also possess clear limitations. Autoregressive models are computationally costly and cannot capture the permutation-invariant nature of graphs, while one-shot generative models based on the likelihood fail to model structural information due to the restriction on the architectures to ensure tractable likelihood computation.

Apart from the likelihood-based methods, Niu et al. (2020) introduced a score-based generative model for graphs, namely, edge-wise dense prediction graph neural network (EDP-GNN). However, since EDP-GNN utilizes the discrete-step perturbation of heuristically chosen noise scales to estimate the score function, both its flexibility and its efficiency are limited. Moreover, EDP-GNN only generates adjacency matrices of graphs, thus is unable to fully capture the node-edge dependency which is crucial for the generation of real-world graphs such as molecules.

To overcome the limitations of previous graph generative models, we propose a novel score-based graph generation framework on a continuous-time domain that can generate both the node features and the adjacency matrix. Specifically, we propose a novel *Graph Diffusion via the System of Stochastic differential equations* (GDSS), which describes the perturbation of both node features and adjacency through a system of SDEs, and show that the previous work of Niu et al. (2020) is a special instance of GDSS. Diffusion via the system of SDEs can be interpreted as the decomposition of the full diffusion into simpler diffusion processes of respective components while modeling the dependency. Further, we derive novel training objectives for the proposed diffu-

sion, which enable us to estimate the gradient of the joint log-density with respect to each component, and introduce a new integrator for solving the proposed system of SDEs.

We experimentally validate our method on generic graph generation tasks by evaluating the generation quality on synthetic and real-world graphs, on which ours outperforms existing one-shot generative models while achieving competitive performance to autoregressive models. We further validate our method on molecule generation tasks, where ours outperforms the state-of-the-art baselines including the autoregressive methods, demonstrating that the proposed diffusion process through the system of SDEs is able to capture the complex dependency between nodes and edges. We summarize our main contributions as follows:

- We propose a novel score-based generative model for graphs that overcomes the limitation of previous generative methods, by introducing a diffusion process for graphs that can generate node features and adjacency simultaneously via the system of SDEs.
- We derive novel training objectives to estimate the gradient of the joint log-density for the proposed diffusion process and further introduce an efficient integrator to solve the proposed system of SDEs.
- We validate our method on both synthetic and real-world graph generation tasks, on which ours outperforms existing graph generative models.

2. Related Work

Score-based Generative Models Score-based generative models generate samples from noise by first perturbing the data with gradually increasing noise, then learning to reverse the perturbation via estimating the score function, which is the gradient of the log-density function with respect to the data. Two representative classes of score-based generative models have been proposed by Song & Ermon (2019) and Ho et al. (2020), respectively. Score matching with Langevin dynamics (SMLD) (Song & Ermon, 2019) estimates the score function at multiple noise scales, then generates samples using annealed Langevin dynamics to slowly decrease the scales. On the other hand, denoising diffusion probabilistic modeling (DDPM) (Ho et al., 2020) backtracks each step of the noise perturbation by considering the diffusion process as a parameterized Markov chain and learning the transition of the chain. Recently, Song et al. (2021b) showed that these approaches can be unified into a single framework, describing the noise perturbation as the forward diffusion process modeled by the stochastic differential equation (SDE). Although score-based generative models have shown successful results for the generation of images (Ho et al., 2020; Song et al., 2021b;a; Dhariwal & Nichol, 2021), audio (Chen et al., 2021; Kong et al., 2021; Jeong et al., 2021; Mittal et al., 2021), and point clouds (Cai

et al., 2020; Luo & Hu, 2021), the graph generation task remains to be underexplored due to the discreteness of the data structure and the complex dependency between nodes and edges. To the best of our knowledge, we are the first to propose a diffusion process for graphs and further model the dependency through a system of SDEs. It is notable that recent developments of score-based generative methods, such as latent score-based generative model (LSGM) (Vahdat et al., 2021) and critically-damped Langevin diffusion (CLD) (Dockhorn et al., 2021), are complementary to our method as we can apply these methods to improve each component-wise diffusion process.

Graph Generative Models The common goal of graph generative models is to learn the underlying distribution of graphs. Graph generative models can be classified into two categories based on the type of the generation process: autoregressive and one-shot. Autoregressive graph generative models include generative adversarial network (GAN) models (You et al., 2018a), recurrent neural network (RNN) models (You et al., 2018b; Popova et al., 2019), variational autoencoder (VAE) models (Jin et al., 2018; 2020), and normalizing flow models (Shi et al., 2020; Luo et al., 2021). Works that specifically focus on the scalability of the generation comprise another branch of autoregressive models (Liao et al., 2019; Dai et al., 2020). Although autoregressive models show state-of-the-art performance, they are computationally expensive and cannot model the permutation-invariant nature of the true data distribution. On the other hand, one-shot graph generative models aim to directly model the distribution of all the components of a graph as a whole, thereby considering the structural dependency as well as the permutation-invariance. One-shot graph generative models can be also further categorized into GAN models (De Cao & Kipf, 2018), VAE models (Ma et al., 2018), and normalizing flow models (Madhawa et al., 2019; Zang & Wang, 2020). There are also recent approaches that utilize energy-based models (EBMs) and score-based models, respectively (Liu et al., 2021b; Niu et al., 2020). Previous one-shot generative models perform poorly due to the restricted model architectures for building a normalized probability, which are insufficient to learn the complex dependency of nodes and edges. To overcome these limitations, we introduce a novel permutation-invariant one-shot generative method based on score-based diffusion model that imposes fewer constraints on the model architecture.

Score-based Graph Generation To the best of our knowledge, the work of Niu et al. (2020) is the only work that approaches graph generation with the score-based generative model. Niu et al. (2020) aims to generate graphs by estimating the score of the adjacency matrices at a finite number of noise scales, and using Langevin dynamics to sample from a series of decreasing noise scales for generation. However,

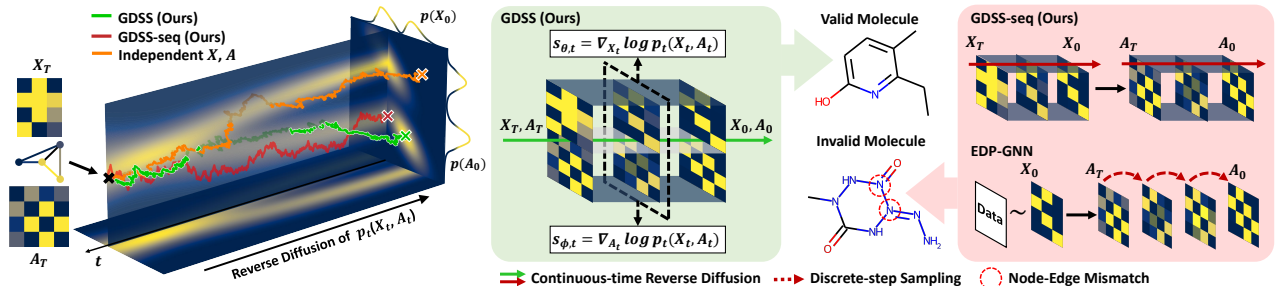


Figure 1: **(Left) Visualization of graph generation through the reverse-time diffusion process.** The colored trajectories denote different types of diffusion processes in the joint probability space of node features \mathbf{X} and adjacency \mathbf{A} . We compare three types of diffusion: GDSS (green) can successfully generate samples from the data distribution by modeling the dependency between the components, whereas GDSS-seq (red) or the independent diffusion of each component (orange) fails. **(Right) Illustration of proposed score-based graph generation framework.** GDSS generates \mathbf{X} and \mathbf{A} simultaneously by modeling the dependency through time, whereas GDSS-seq generates them sequentially. EDP-GNN generates only \mathbf{A} with \mathbf{X} sampled from the training data. Note that GDSS and GDSS-seq are based on a continuous-time diffusion process, while EDP-GNN is based on a discrete-step perturbation procedure.

Langevin dynamics requires numerous sampling steps for each noise scale, thereby having difficulty for generating large-scale graphs. Furthermore, Niu et al. (2020) focus on the generation of adjacency without the generation of node features, resulting in suboptimal learning of the distributions of node-attributed graphs such as molecular graphs. A naive extension of the work of Niu et al. (2020) that generates the node features and the adjacency either simultaneously or alternately will still be suboptimal since it cannot capture the complex dependency between the nodes and edges. Therefore, we propose a novel score-based generative framework for graphs that can interdependently generate the nodes and edges. Specifically, we propose a novel diffusion process for graphs via a system of SDEs that smoothly transforms the data distribution to known prior and vice versa, which overcomes the limitation of the discrete-step perturbation procedure used in Song & Ermon (2020).

3. Graph Diffusion via the System of SDEs

In this section, we introduce our novel continuous-time score-based generative framework for modeling graphs using the system of SDEs. We first explain our proposed graph diffusion process via a system of SDEs in Section 3.1, then derive new objectives for estimating the gradients of the joint log-density with respect to each component in Section 3.2. Finally, we present an effective method for solving the system of reverse-time SDEs in Section 3.3.

3.1. Graph Diffusion Process

The goal of graph generation is to synthesize graphs that closely follow the distribution of the observed set of graphs. To bypass the difficulty of directly representing the distribution, we introduce a continuous-time score-based generative framework for graph generation. Specifically, we propose a novel graph diffusion process through the system of SDEs that models the dependency between the nodes and edges

of a graph. We begin by explaining the proposed forward diffusion process for graphs.

A graph \mathcal{G} with N nodes is defined by its node features $\mathbf{X} \in \mathbb{R}^{N \times F}$ and the weighted adjacency matrix $\mathbf{A} \in \mathbb{R}^{N \times N}$ as $\mathcal{G} = (\mathbf{X}, \mathbf{A}) \in \mathbb{R}^{N \times F} \times \mathbb{R}^{N \times N} := \mathcal{G}$, where F is the dimension of the node features. To model the dependency between \mathbf{X} and \mathbf{A} , we propose a forward diffusion process of graphs that transforms both the node features and the adjacency matrix to a simple noise distribution. Formally, the diffusion process can be represented as $\{\mathbf{G}_t = (\mathbf{X}_t, \mathbf{A}_t)\}_{t=0}^T$ with a continuous time variable $t \in [0, T]$ where $\mathbf{G}_0 \sim p_{data}$ and $\mathbf{G}_T \sim p_T$, and p_{data} and p_T are the data distribution and the prior distribution, respectively. The process can be described by the Itô SDE:

$$d\mathbf{G}_t = \mathbf{f}_t(\mathbf{G}_t)dt + \mathbf{g}_t(\mathbf{G}_t)d\mathbf{w}, \quad (1)$$

where $\mathbf{f}_t(\cdot): \mathcal{G} \rightarrow \mathcal{G}^1$ is the linear drift coefficient, $\mathbf{g}_t: \mathcal{G} \rightarrow \mathcal{G} \times \mathcal{G}$ is the diffusion coefficient, and \mathbf{w} is the standard Wiener process. The coefficients \mathbf{f} and \mathbf{g} are designed to guarantee $\mathbf{G}_T \sim p_T$, where the prior distribution p_T has a tractable form to efficiently generate samples. For ease of presentation, we define $\mathbf{g}_t(\mathbf{G}_t)$ to be a scalar function g_t . Note that ours is the first work that proposes a diffusion process for generating a whole graph consisting of nodes and edges, in that the work of Niu et al. (2020) (1) utilizes the finite-step perturbation and (2) only perturbs the adjacency matrix with fixed node features sampled from training data.

From the proposed diffusion process, we can generate samples by starting from the prior distribution and reversing Eq. (1) in time, which is also a diffusion process described by the following reverse-time SDE (Anderson, 1982; Song et al., 2021b):

$$d\mathbf{G}_t = [\mathbf{f}_t(\mathbf{G}_t) - g_t^2 \nabla_{\mathbf{G}_t} \log p_t(\mathbf{G}_t)] d\tilde{t} + g_t d\tilde{\mathbf{w}}, \quad (2)$$

¹We use the t -subscript to represent functions of time: $F_t(\cdot) := F(\cdot, t)$ and $\mathbf{M}_{\theta,t}(\cdot) := \mathbf{M}_{\theta}(\cdot, t)$.

where $\bar{\mathbf{w}}$ is a reverse-time standard Wiener process and $d\bar{t}$ is an infinitesimal negative time step. However, solving Eq. (2) directly requires the estimation of high-dimensional score $\nabla_{\mathbf{G}_t} \log p_t(\mathbf{G}_t) \in \mathbb{R}^{N \times F} \times \mathbb{R}^{N \times N}$, which is expensive to compute. To bypass this computation, we propose a novel reverse-time diffusion process equivalent to Eq. (2), modeled by the following system of SDEs:

$$\begin{cases} d\mathbf{X}_t = [\mathbf{f}_{1,t}(\mathbf{X}_t) - g_{1,t}^2 \nabla_{\mathbf{X}_t} \log p_t(\mathbf{X}_t, \mathbf{A}_t)] d\bar{t} + g_{1,t} d\bar{\mathbf{w}}_1 \\ d\mathbf{A}_t = [\mathbf{f}_{2,t}(\mathbf{A}_t) - g_{2,t}^2 \nabla_{\mathbf{A}_t} \log p_t(\mathbf{X}_t, \mathbf{A}_t)] d\bar{t} + g_{2,t} d\bar{\mathbf{w}}_2, \end{cases} \quad (3)$$

where $\mathbf{f}_{1,t}$ and $\mathbf{f}_{2,t}$ satisfy $\mathbf{f}_t(\mathbf{X}, \mathbf{A}) = (\mathbf{f}_{1,t}(\mathbf{X}), \mathbf{f}_{2,t}(\mathbf{A}))$, $g_t = (g_{1,t}, g_{2,t})$, and $\bar{\mathbf{w}}_1, \bar{\mathbf{w}}_2$ are reverse-time standard Wiener processes. We refer to these forward and reverse diffusion processes as *Graph Diffusion via the System of SDEs* (GDSS). Note that each SDE in Eq. (3) describes the diffusion process for each component, \mathbf{X} and \mathbf{A} , respectively, thus we may perceive the reverse diffusion of a graph as the reverse diffusion of each component through time. The key property of GDSS is that the SDEs in the system are dependent on each other, related by the gradients of the joint log-density which we refer to as the *partial score functions*. Due to the partial scores, GDSS is able to model the dependency between the components through time. To demonstrate the importance of modeling the dependency, we present two variants of our proposed GDSS and compare their generative performance.

The first variant is the continuous-time version of EDP-GNN (Niu et al., 2020). By ignoring the diffusion process of \mathbf{X} in Eq. (3) with $\mathbf{f}_{1,t} = g_{1,t} = 0$ and choosing the prior distribution of \mathbf{X} as the data distribution, we obtain a diffusion process of \mathbf{A} that generalizes the discrete-step noise perturbation procedure of EDP-GNN. Therefore, EDP-GNN can be considered as a special example of GDSS without the diffusion process of the node features, which further replaces the diffusion by the discrete-step perturbation with a finite number of noise scales. We present another variant of GDSS that generates \mathbf{X} and \mathbf{A} sequentially instead of generating them simultaneously. By neglecting some part of the dependency through the assumptions $\nabla_{\mathbf{X}_t} \log p_t(\mathbf{X}_t, \mathbf{A}_t) \approx \nabla_{\mathbf{X}_t} \log p_t(\mathbf{X}_t)$ and $\nabla_{\mathbf{A}_t} \log p_t(\mathbf{X}_t, \mathbf{A}_t) \approx \nabla_{\mathbf{A}_t} \log p_t(\mathbf{X}_0, \mathbf{A}_t)$, we can derive the following SDEs for the diffusion process of the variant:

$$\begin{cases} d\mathbf{X}_t = [\mathbf{f}_{1,t}(\mathbf{X}_t) - g_{1,t}^2 \nabla_{\mathbf{X}_t} \log p_t(\mathbf{X}_t)] d\bar{t} + g_{1,t} d\bar{\mathbf{w}}_1 \\ d\mathbf{A}_t = [\mathbf{f}_{2,t}(\mathbf{A}_t) - g_{2,t}^2 \nabla_{\mathbf{A}_t} \log p_t(\mathbf{X}_0, \mathbf{A}_t)] d\bar{t} + g_{2,t} d\bar{\mathbf{w}}_2, \end{cases} \quad (4)$$

which are sequential in the sense that the reverse diffusion process of \mathbf{A} is determined by \mathbf{X}_0 , the result of the reverse diffusion of \mathbf{X} . Thus simulating Eq. (4) can be interpreted as generating the node features \mathbf{X} first, then generating the adjacency \mathbf{A} sequentially, which we refer to as *GDSS-seq*.

The reverse diffusion process of these two variants, EDP-GNN and GDSS-seq, are visualized in Figure 1 as the red

trajectory in the joint (\mathbf{X}, \mathbf{A}) -space, where the trajectory is constrained to the hyperplane defined by $\mathbf{X}_t = \mathbf{X}_0$, thereby do not fully reflect the dependency. On the other hand, GDSS represented as the green trajectory is able to diffuse freely from the noise to the data distribution by modeling the joint distribution through the system of SDEs, successfully generating samples from the data distribution.

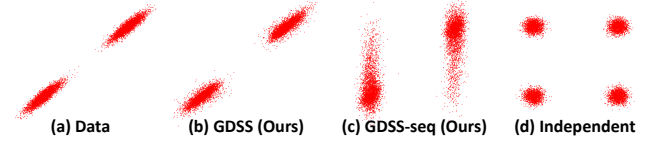


Figure 2: **A toy experiment on modeling the dependency.** GDSS successfully models the correlation, whereas others fail. See Appendix C.2 for more details of the experiment.

To empirically verify this observation, we conduct a simple experiment where the data distribution is a bivariate Gaussian mixture. The generated samples of each method are shown in Figure 2. While GDSS successfully represents the correlation of the two variables, GDSS-seq fails to capture their covariance and generates samples that deviate from the data distribution. We observe that EDP-GNN shows a similar result. We further extensively validate the effectiveness of our GDSS in modeling the dependency in Section 4.

Note that once the partial scores $\nabla_{\mathbf{X}_t} \log p_t(\mathbf{X}_t, \mathbf{A}_t)$ and $\nabla_{\mathbf{A}_t} \log p_t(\mathbf{X}_t, \mathbf{A}_t)$ in Eq. (3) are known for all t , the reverse-time process can be used as a generative model. In order to estimate the partial scores with neural networks, we introduce novel training objectives for GDSS in the following subsection.

3.2. Estimating the Partial Score Functions

Score Matching Objectives One approach for estimating the partial score functions is to adopt the continuous generalization of score matching objectives (Hyvärinen, 2005; Song et al., 2021b) to train the time-dependent score-based models $\mathbf{s}_{\theta,t}$ and $\mathbf{s}_{\phi,t}$ as follows:

$$\begin{aligned} & \min_{\theta} \mathbb{E}_t \left\{ \lambda_t \mathbb{E}_{\mathbf{G}_0} \mathbb{E}_{\mathbf{G}_t | \mathbf{G}_0} \|\mathbf{s}_{\theta,t}(\mathbf{G}_t) - \nabla_{\mathbf{X}_t} \log p_t(\mathbf{G}_t)\|_2^2 \right\} \\ & \min_{\phi} \mathbb{E}_t \left\{ \lambda_t \mathbb{E}_{\mathbf{G}_0} \mathbb{E}_{\mathbf{G}_t | \mathbf{G}_0} \|\mathbf{s}_{\phi,t}(\mathbf{G}_t) - \nabla_{\mathbf{A}_t} \log p_t(\mathbf{G}_t)\|_2^2 \right\}, \end{aligned} \quad (5)$$

where $\lambda_t: [0, T] \rightarrow \mathbb{R}$ is a positive weighting function for uniformly sampled $t \sim \mathcal{U}[0, T]$, \mathbf{G}_0 is a sample from the data distribution p_{data} , and \mathbf{G}_t is a sample from the transition kernel $p_{0t}(\mathbf{G}_t | \mathbf{G}_0)$ determined by the forward diffusion process. However, we cannot train directly with Eq. (5) since the joint distribution $p_t(\mathbf{X}_t, \mathbf{A}_t)$ is not analytically accessible in general. Thereby we search for tractable score matching objectives for estimating the partial scores $\nabla_{\mathbf{X}_t} \log p_t(\mathbf{X}_t, \mathbf{A}_t)$ and $\nabla_{\mathbf{A}_t} \log p_t(\mathbf{X}_t, \mathbf{A}_t)$.

We start by introducing equivalent objectives employing the denoising score matching (Song & Ermon, 2019; Song et al.,

2021b) with respect to the gradient of each \mathbf{X}_t and \mathbf{A}_t (see Appendix A.1 for the derivation):

$$\begin{aligned} & \min_{\theta} \mathbb{E}_t \left\{ \lambda_t \mathbb{E}_{\mathbf{G}_0} \mathbb{E}_{\mathbf{G}_t | \mathbf{G}_0} \left\| \mathbf{s}_{\theta,t}(\mathbf{G}_t) - \nabla_{\mathbf{X}_t} \log p_{0t}(\mathbf{G}_t | \mathbf{G}_0) \right\|_2^2 \right\} \\ & \min_{\phi} \mathbb{E}_t \left\{ \lambda_t \mathbb{E}_{\mathbf{G}_0} \mathbb{E}_{\mathbf{G}_t | \mathbf{G}_0} \left\| \mathbf{s}_{\phi,t}(\mathbf{G}_t) - \nabla_{\mathbf{A}_t} \log p_{0t}(\mathbf{G}_t | \mathbf{G}_0) \right\|_2^2 \right\}. \end{aligned}$$

From the forward diffusion process in Eq. (1), the transition kernel $p_{0t}(\mathbf{G}_t | \mathbf{G}_0)$ can be separated in terms of \mathbf{X}_t and \mathbf{A}_t :

$$p_{0t}(\mathbf{G}_t | \mathbf{G}_0) = p_{0t}(\mathbf{X}_t | \mathbf{X}_0) p_{0t}(\mathbf{A}_t | \mathbf{A}_0). \quad (6)$$

Notably, each kernel $p_{0t}(\mathbf{X}_t | \mathbf{X}_0)$ and $p_{0t}(\mathbf{A}_t | \mathbf{A}_0)$ is a Gaussian distribution with closed form mean and variance, determined by the coefficients \mathbf{f}_t and \mathbf{g}_t . Using the result of Eq. (6), we propose new training objectives which are equivalent to the original score matching objectives in Eq. (5) (see Appendix A.2 for the detailed derivation):

$$\begin{aligned} & \min_{\theta} \mathbb{E}_t \left\{ \lambda_t \mathbb{E}_{\mathbf{G}_0} \mathbb{E}_{\mathbf{G}_t | \mathbf{G}_0} \left\| \mathbf{s}_{\theta,t}(\mathbf{G}_t) - \nabla_{\mathbf{X}_t} \log p_{0t}(\mathbf{X}_t | \mathbf{X}_0) \right\|_2^2 \right\} \\ & \min_{\phi} \mathbb{E}_t \left\{ \lambda_t \mathbb{E}_{\mathbf{G}_0} \mathbb{E}_{\mathbf{G}_t | \mathbf{G}_0} \left\| \mathbf{s}_{\phi,t}(\mathbf{G}_t) - \nabla_{\mathbf{A}_t} \log p_{0t}(\mathbf{A}_t | \mathbf{A}_0) \right\|_2^2 \right\}. \end{aligned} \quad (7)$$

The expectations in Eq. (7) can be computed using the Monte Carlo estimate with the samples $\{(t, \mathbf{G}_0, \mathbf{G}_t)\}$. Note that estimating the partial scores is not equivalent to estimating $\nabla_{\mathbf{X}_t} \log p_t(\mathbf{X}_t)$ or $\nabla_{\mathbf{A}_t} \log p_t(\mathbf{A}_t)$, the main objective of previous score-based generative models, since estimating the former requires capturing the dependency between \mathbf{X}_t and \mathbf{A}_t determined by the joint probability. With these training objectives, we can effectively estimate the partial scores using the time-dependent score-based models which we describe in the next paragraph.

Permutation-equivariant Score-based Model Another essential step to estimate the partial score functions is to design the appropriate score-based models. We propose a new architecture for the time-dependent score-based models that can capture the joint distribution of \mathbf{X} and \mathbf{A} based on graph neural networks (GNNs). To estimate $\nabla_{\mathbf{A}_t} \log p_t(\mathbf{X}_t, \mathbf{A}_t)$, we utilize the graph multi-head attention (Baek et al., 2021) to distinguish important relations between nodes, while using the higher-order adjacency matrices to represent the long-range dependencies between them as follows:

$$\mathbf{s}_{\phi}(\mathbf{G}_t) = \text{MLP} \left(\left[\left\{ \text{GMH}(\mathbf{H}_i, \mathbf{A}_i^p) \right\}_{i=0, p=1}^{K, P} \right] \right), \quad (8)$$

where \mathbf{A}_i^p are the higher-order adjacency matrices, $\mathbf{H}_{i+1} = \text{GNN}(\mathbf{H}_i, \mathbf{A}_i)$ with $\mathbf{H}_0 = \mathbf{X}_t$ given, $[\cdot]$ denotes the concatenation operation and GMH denotes the graph multi-head attention block. Further, we introduce the following model to estimate $\nabla_{\mathbf{X}_t} \log p_t(\mathbf{X}_t, \mathbf{A}_t)$:

$$\mathbf{s}_{\theta}(\mathbf{G}_t) = \text{MLP} \left(\left[\left\{ \mathbf{H}_i \right\}_{i=0}^L \right] \right), \quad (9)$$

where $\mathbf{H}_{i+1} = \text{GNN}(\mathbf{H}_i, \mathbf{A}_i)$ with $\mathbf{H}_0 = \mathbf{X}_t$ given. Following Song & Ermon (2020), we incorporate the time information to the model by rescaling the output of the score model with the standard deviation of the transition kernel.

Note that since the message-passing operations of GNNs and the attention function used in GMH are permutation-equivariant (Keriven & Peyré, 2019), the proposed score-based models are also permutation-equivariant, and the log-likelihood implicitly defined by $\mathbf{s}_{\theta,t}$ and $\mathbf{s}_{\phi,t}$ is guaranteed to be permutation-invariant (Niu et al., 2020).

3.3. Solving the System of Reverse-time SDEs

To use the reverse-time process as a generative model, it requires to simulate the following system of reverse-time SDEs estimated by the score models:

$$\begin{cases} d\mathbf{X}_t = \underbrace{\mathbf{f}_{1,t}(\mathbf{X}_t)}_F dt + g_{1,t} d\bar{\mathbf{w}}_1 - g_{1,t}^2 \mathbf{s}_{\theta,t}(\mathbf{X}_t, \mathbf{A}_t) d\bar{t} \\ d\mathbf{A}_t = \underbrace{\mathbf{f}_{2,t}(\mathbf{A}_t)}_F dt + g_{2,t} d\bar{\mathbf{w}}_2 - g_{2,t}^2 \mathbf{s}_{\phi,t}(\mathbf{X}_t, \mathbf{A}_t) d\bar{t} \end{cases} \quad (10)$$

However, solving the system of two diffusion processes that are tied by the partial scores brings about another difficulty. Thus we propose a novel integrator, *Symmetric Splitting for System of SDEs* (S4) that is efficient yet accurate, inspired by the Symmetric Splitting CLD Sampler (SSCS) (Dockhorn et al., 2021) and Predictor-Corrector Sampler (PC sampler) (Song et al., 2021b).

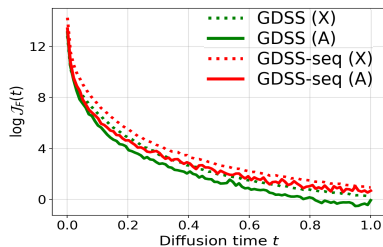
Specifically, at each discretized time step t , S4 consists of three steps: the score computation, the prediction, and the correction. First, S4 computes the partial scores with given estimation of \mathbf{X}_t and \mathbf{A}_t using the score models $\mathbf{s}_{\theta,t}$ and $\mathbf{s}_{\phi,t}$, where the computed partial scores are later used for both the prediction and the correction steps. Then, we employ Langevin MCMC (Parisi, 1981) in order to calibrate the estimated sample \mathbf{G}_t , with the precomputed partial scores. The remaining step is to predict the solution for the next time step δt , which we approach by approximating the intractable solution of Eq. (10) using the classical propagator $e^{t(\hat{\mathcal{L}}_F^* + \hat{\mathcal{L}}_S^*)}$, where the action of Fokker-Planck operators $\hat{\mathcal{L}}_F^*$ and $\hat{\mathcal{L}}_S^*$ corresponds to the forward diffusion term F and score model term S in Eq. (10), respectively (see Appendix A.3 for the detailed derivation). From the symmetric Trotter theorem (Trotter, 1959; Strang, 1968), we are able to approximate the intractable solution by evaluating the action of $e^{\frac{\delta t}{2} \hat{\mathcal{L}}_F^*}$ and $e^{\delta t \hat{\mathcal{L}}_S^*}$ successively. The action of $e^{\frac{\delta t}{2} \hat{\mathcal{L}}_F^*}$ describes the reverse-time SDEs of the F term in Eq. (10), which is equal to sampling from the transition kernel of the forward process diffusion in Eq. (1) as follows (see Appendix A.4 for the derivation of the transition kernel):

$$e^{\frac{\delta t}{2} \hat{\mathcal{L}}_F^*} \mathbf{G}_t \sim p_{t, t-\delta t/2}(\mathbf{G}_{t-\delta t/2} | \mathbf{G}_t). \quad (11)$$

On the other hand, the action of $e^{\delta t \hat{\mathcal{L}}_S^*}$ is not analytically

Table 1: **Generation results on the generic graph datasets.** We report the MMD distances between the test datasets and generated graphs. Best results are highlighted in bold (smaller the better). The results of the baselines for Ego-small and Community-small dataset are taken from Niu et al. (2020) and Luo et al. (2021). Hyphen (-) denotes out-of-resources that take more than 10 days or not applicable due to the memory issue. * denotes our own implementation and † indicates unreproducible results. Due to the space limitation, we provide the standard deviations in Appendix D.1.

		Ego-small				Community-small				Enzymes				Grid			
		Real, $4 \leq V \leq 18$				Synthetic, $12 \leq V \leq 20$				Real, $10 \leq V \leq 125$				Synthetic, $100 \leq V \leq 400$			
		Deg.	Clus.	Orbit	Avg.	Deg.	Clus.	Orbit	Avg.	Deg.	Clus.	Orbit	Avg.	Deg.	Clus.	Orbit	Avg.
Autoreg.	DeepGMG	0.040	0.100	0.020	0.053	0.220	0.950	0.400	0.523	-	-	-	-	-	-	-	-
	GraphRNN	0.090	0.220	0.003	0.104	0.080	0.120	0.040	0.080	0.017	0.062	0.046	0.042	0.064	0.043	0.021	0.043
	GraphAF*	0.03	0.11	0.001	0.047	0.18	0.20	0.02	0.133	1.669	1.283	0.266	1.073	-	-	-	-
	GraphDF*	0.04	0.13	0.01	0.060	0.06	0.12	0.03	0.070	1.503	1.061	0.202	0.922	-	-	-	-
One-shot	GraphVAE*	0.130	0.170	0.050	0.117	0.350	0.980	0.540	0.623	1.369	0.629	0.191	0.730	1.619	0.0	0.919	0.846
	GNF†	0.030	0.100	0.001	0.044	0.200	0.200	0.110	0.170	-	-	-	-	-	-	-	-
	EDP-GNN	0.052	0.093	0.007	0.051	0.053	0.144	0.026	0.074	0.023	0.268	0.082	0.124	0.455	0.238	0.328	0.340
	GDSS-seq (Ours)	0.032	0.027	0.011	0.023	0.090	0.123	0.007	0.073	0.099	0.225	0.010	0.111	0.171	0.011	0.223	0.135
	GDSS (Ours)	0.021	0.024	0.007	0.017	0.045	0.086	0.007	0.046	0.026	0.061	0.009	0.032	0.111	0.005	0.070	0.062



Solver	Community-small				Enzymes			
	Deg.	Clus.	Orbit	Time (s)	Deg.	Clus.	Orbit	Time (s)
EM	0.055	0.133	0.017	29.64	0.060	0.581	0.120	153.58
Reverse	0.058	0.125	0.016	29.75	0.057	0.550	0.112	155.06
EM + Langevin	0.045	0.086	0.007	59.93	0.028	0.062	0.010	308.42
Rev. + Langevin	0.045	0.086	0.007	59.40	0.028	0.064	0.009	310.35
S4 (Ours)	0.042	0.101	0.007	30.93	0.026	0.061	0.009	157.57

Figure 3: (Left) **Complexity of the score networks** measured by the Frobenius norm of Jacobian of the neural network. We compare GDSS (green) against GDSS-seq (red), where the solid and dotted lines denote the networks estimating the partial scores with respect to \mathbf{X} and \mathbf{A} , respectively. (Right) **Comparison between fixed step size SDE solvers.** We measure the time for generation of 128 graphs.

tractable. Thus we approximate the action with simple Euler method for solving the ODE corresponding to the score model term S in Eq. (10), using the precomputed partial scores, which is possible due to the action of $e^{\frac{\delta t}{2} \hat{\mathcal{L}}_F^*}$ on sufficiently small half-step $\delta t/2$. By using the Euler method, the prediction step has the same order of error as EM with local error $\mathcal{O}(\delta t^2)$ and global error $\mathcal{O}(\delta t)$ (Dockhorn et al., 2021). We provide the pseudo-code for the S4 solver in Algorithm 1 of Appendix. Although S4 and PC sampler both carry out the prediction and correction steps, S4 solver is far more efficient since S4 requires half the number of forward passes of score models to that of the PC sampler, which dominates the computational cost of solving the SDEs. To obtain a more accurate solution with the cost of computation, one might consider using a higher-order integrator such Runge-Kutta method to approximate $e^{\delta t \hat{\mathcal{L}}_S^*}$, while using HMC (Neal, 2012) for the correction step. Note that the proposed S4 can be used to solve a general system of SDEs, including the system with mixed types of SDEs such as those of VPSDE and VESDE (Song et al., 2021b), whereas SSCS is limited to solving a specific type of SDE, namely CLD.

4. Experiments

We experimentally validate the performance of our method in generation of generic graphs as well as molecular graphs.

4.1. Generic Graph Generation

Experimental Setup We first validate GDSS by evaluating the quality of the generated samples on four generic graph datasets, including synthetic and real-world graphs with varying sizes: (1) Ego-small, 200 small ego graphs drawn from larger Citeseer network dataset (Sen et al., 2008), (2) Community-small, 100 randomly generated community graphs, (3) Enzymes, 587 protein graphs which represent the protein tertiary structures of the enzymes from the BRENDA database (Schomburg et al., 2004), (4) Grid, 100 standard 2D grid graphs. The detailed statistics of each dataset are in Table 1. For a fair comparison, we follow the experimental and evaluation setting of You et al. (2018b) and use the same train/test split. We use the maximum mean discrepancy (MMD) to compare the distributions of graph statistics between the same number of generated and test graphs. Following You et al. (2018b), we measure the distributions of degree, clustering coefficient, and the number of occurrences of orbits with 4 nodes. Note that we use the Gaussian Earth Mover’s Distance (EMD) kernel to compute the MMDs instead of the total variation (TV) distance used in Liao et al. (2019), since the TV distance leads to an indefinite kernel and an undefined behavior (O’Bray et al., 2021). See Appendix C.3 for more details.

Baselines We compare our proposed method against the following deep generative models. **GraphVAE** (Simonovskiy & Komodakis, 2018) is a one-shot VAE-based

Table 2: **Generation results on the QM9 and ZINC250k dataset.** Results are the means of 3 runs. Values denoted by * are taken from the respective original papers. Other results are obtained by running open-source codes. Best results are highlighted in bold. Val. w/o corr. denotes the Validity w/o correction metric, and values that do not exceed 50% are underlined. Due to the space limitation, we provide the results of validity, uniqueness, and novelty as well as the standard deviations in Appendix D.2.

Method	QM9				ZINC250k				
	Val. w/o corr.↑	NSPDK↓	FCD↓	Time (s)↓	Val. w/o corr.↑	NSPDK↓	FCD↓	Time (s)↓	
Autoreg.	GraphAF (Shi et al., 2020)	67*	0.020	5.268	2.52e ³	68*	0.044	16.289	5.80e ³
	GraphAF+FC	74.43	0.021	5.625	2.55e ³	68.47	0.044	16.023	6.02e ³
	GraphDF (Luo et al., 2021)	82.67*	0.063	10.816	5.35e ⁴	89.03*	0.176	34.202	6.03e ⁴
	GraphDF+FC	93.88	0.064	10.928	4.91e ⁴	90.61	0.177	33.546	5.54e ⁴
One-shot	MoFlow (Zang & Wang, 2020)	91.36	0.017	4.467	4.60	63.11	0.046	20.931	2.45e¹
	EDP-GNN (Niu et al., 2020)	<u>47.52</u>	0.005	2.680	4.40e ³	82.97	0.049	16.737	9.09e ³
	GraphEBM (Liu et al., 2021b)	<u>8.22</u>	0.030	6.143	3.71e ¹	<u>5.29</u>	0.212	35.471	5.46e ¹
	GDSS-seq (Ours)	94.47	0.010	4.004	1.13e ²	92.39	0.030	16.847	2.02e ³
	GDSS (Ours)	95.72	0.003	2.900	1.14e ²	97.01	0.019	14.656	2.02e ³

	Train	GDSS (Ours)	GDSS-seq (Ours)	GraphAF	MoFlow	GraphDF	EDP-GNN	GraphEBM
QM9								
		0.5600	0.2857	0.2581	0.2857	0.1818	0.3448	0.2500
ZINC250k								
		0.5000	0.2714	0.3846	0.3099	0.1500	0.2769	0.1867

Figure 4: **Visualization of generated molecules with maximum Tanimoto similarity** to the molecule from the dataset. The top row shows QM9 molecules while the bottom row shows ZINC250k molecules. For each generated molecule, we display the similarity value at the bottom. The pairwise Tanimoto similarity is calculated based on the standard Morgan fingerprints with radius 2 and 1024 bits.

model. **DeepGMG** (Li et al., 2018a) and **GraphRNN** (You et al., 2018b) are autoregressive RNN-based models. **GNF** (Liu et al., 2019) is a one-shot flow-based model. **GraphAF** (Shi et al., 2020) is an autoregressive flow-based model. **EDP-GNN** (Niu et al., 2020) is a one-shot score-based model. **GraphDF** (Luo et al., 2021) is an autoregressive flow-based model that utilizes discrete latent variables. For GDSS, we generate samples either using EM, PC sampler, or the proposed S4 solver.

Results Table 1 shows that the proposed GDSS significantly outperforms all the baseline one-shot generative models including EDP-GNN, and also outperforms the autoregressive baselines on most of the datasets except Grid. Moreover, GDSS shows competitive performance to the state-of-the-art autoregressive model GraphRNN on generating large graphs in the Grid dataset, for which GDSS is the only method that achieves similar performance. We observe that EDP-GNN, a previous score-based generation model for graphs, completely fails in generating large graphs. We further visualize the generated graphs of GDSS and baselines in Appendix E.1, which shows that GDSS properly captures the distinct topological structures of the target graphs, thanks to its ability to model the dependency which we analyze further in Section 4.3.

Complexity of Learning the Partial Scores Learning the partial score function $\nabla_{\mathbf{A}_t} \log p_t(\mathbf{X}_t, \mathbf{A}_t)$ regarding both \mathbf{X} and \mathbf{A} may seem difficult compared to learning

the function $\nabla_{\mathbf{A}_t} \log p_t(\mathbf{X}_0, \mathbf{A}_t)$ that concerns only \mathbf{A} . We empirically demonstrate this is not the case, by measuring the complexity of the score networks that estimate the partial scores. The complexity of the models can be measured via the squared Frobenius norm of their Jacobians $\mathcal{J}_F(t)$, and we compare the score models of GDSS and GDSS-seq trained with the Ego-small dataset. As shown in Figure 3, the complexity of GDSS estimating $\nabla_{\mathbf{A}_t} \log p_t(\mathbf{X}_t, \mathbf{A}_t)$ is significantly smaller compared to the complexity of GDSS-seq estimating $\nabla_{\mathbf{A}_t} \log p_t(\mathbf{X}_0, \mathbf{A}_t)$, and similarly for \mathbf{X} . The result stresses the importance of modeling the node-edge dependency, since whether to model the dependency is the only difference between GDSS and GDSS-seq. Further, the reduced complexity with our GDSS further enables efficient generation of large-scale graphs, as demonstrated by the quality of the generated samples for Grid in Table 1.

4.2. Molecule Generation

To show that our method is able to capture the complex dependency between nodes and edges, we further evaluate GDSS on molecule graph generation tasks.

Experimental Setup We use two molecular datasets, QM9 (Ramakrishnan et al., 2014) and ZINC250k (Irwin et al., 2012), where we provide the statistics in Table 4 in Appendix C.4. We examine the quality of the 10,000 generated molecules with the following metrics. **Fréchet ChemNet Distance (FCD)** (Preuer et al., 2018) evaluates the distance

between the training and generated sets using activations of the penultimate layer of a ChemNet. **Neighborhood sub-graph pairwise distance kernel (NSPDK) MMD** (Costa & De Grave, 2010) is the MMD between the generated molecules and test molecules which takes into account both the node and edge features for evaluation. Note that FCD and NSPDK MMD are crucial metrics that assess the ability of a model to learn the distribution of training molecules, measuring how close the generated molecules lie to the distribution. Specifically, FCD measures the ability in the view of molecules, while NSPDK MMD measures the ability in the view of the graph structure. **Validity w/o correction** is the fraction of valid molecules without valency correction or edge resampling, which is different from the one used in Shi et al. (2020) and Luo et al. (2021), since we allow atoms to have formal charge when checking their valency following Zang & Wang (2020), which is more reasonable due to the existence of formal charge in the training molecules. **Time** measures the time for generating 10,000 molecules in the form of RDKit (Landrum et al., 2016) molecules. We provide more details in Appendix C.4.

Baselines We compare our model against the following baselines. **GraphAF** (Shi et al., 2020) is an autoregressive flow-based model. **MoFlow** (Zang & Wang, 2020) is a one-shot flow-based model. **GraphDF** (Luo et al., 2021) is an autoregressive flow-based model using discrete latent variables. **GraphEBM** (Liu et al., 2021b) is a one-shot energy-based model that generates molecules by minimizing energies with Langevin dynamics. We also construct modified versions of GraphAF and GraphDF that consider formal charge (**GraphAF+FC** and **GraphDF+FC**) for a fair comparison with the baselines and ours.

Results As shown in Table 2, GDSS achieves the highest validity when the post-hoc valency correction is disabled, demonstrating that GDSS is able to proficiently learn the chemical valency rule that requires capturing the node-edge relationship. Moreover, GDSS significantly outperforms all the baselines in NSPDK MMD and most of the baselines in FCD, showing that the generated molecules of GDSS lie close to the data distribution both in the space of graphs and the chemical space, and further verify the effectiveness of our method for learning the underlying distribution of graphs with multiple nodes and edge types. We further visualize the generated molecules in Figure 4 and Figure 7 of Appendix D.2, which shows that GDSS is capable of generating molecules that share a large substructure with the molecules in the training set, whereas the generated molecules of the baselines share a smaller structural portion or even completely differ from the training molecules.

Time Efficiency To validate the practicality of GDSS, we compare the inference time of generating molecules with the baselines. As shown in Table 2, GDSS not only outperforms

the autoregressive models in terms of the generation quality, but also in terms of time efficiency. Moreover, GDSS and GDSS-seq require significantly smaller generation time compared to EDP-GNN, showing that representing the transformation of graphs to noise and vice-versa as the diffusion process in the continuous-time framework is more efficient than the discrete-step perturbation used in EDP-GNN.

4.3. Ablation Studies

We provide extensive analysis of the proposed GDSS framework in two different perspectives: (1) The necessity of modeling the dependency between \mathbf{X} and \mathbf{A} , and (2) the effectiveness of the S4 solver.

Necessity of Dependency Modeling To validate that modeling the node-edge dependency is crucial for graph generation, we compare our proposed methods GDSS and GDSS-seq, since the only difference is that the latter only models the dependency of \mathbf{A} on \mathbf{X} (Eq. (3) and Eq. (4)). From the results in Table 1 and Table 2, we observe that GDSS constantly outperforms GDSS-seq in all metrics, proving that accurately learning the distributions of graphs requires modeling the dependency. Moreover, for molecule generation, the dependency can be directly measured in terms of validity, which shows the effectiveness of modeling the dependency via the system of SDEs as in GDSS.

Comparison of SDE Solvers To validate the effectiveness of the proposed S4 solver, we compare its performance against the non-adaptive stepsize solvers, namely EM and Reverse sampler which are predictor-only methods, and PC samplers using Langevin MCMC. As shown in Table 3, S4 significantly outperforms the predictor-only methods, and further outperforms the PC samplers with half the computation time, due to fewer evaluations of the score models.

5. Conclusion

We presented a novel score-based generative framework for learning the underlying distribution of the graphs, which overcomes the limitations of previous graph generative methods. Specifically, we proposed a novel *graph diffusion process via the system of SDEs* that transforms both the node features and adjacency to noise and vice-versa, modeling the dependency between them. Further, we derived new training objectives to estimate the gradients of the joint log-density with respect to each component, and presented a novel integrator to efficiently solve the system of SDEs describing the reverse diffusion process. We validated GDSS on the generation of diverse synthetic and real-world graphs including molecules, on which ours outperforms existing generative methods. We pointed out that modeling the dependency between nodes and edges is crucial for learning the distribution of graphs and shed new light on the effectiveness of score-based generative methods for graphs.

References

- Anderson, B. D. Reverse-time diffusion equation models. *Stochastic Processes and their Applications*, 12(3):313–326, 1982.
- Baek, J., Kang, M., and Hwang, S. J. Accurate learning of graph representations with graph multiset pooling. In *9th International Conference on Learning Representations, ICLR 2021, Virtual Event, Austria, May 3-7, 2021*. OpenReview.net, 2021.
- Brockschmidt, M., Allamanis, M., Gaunt, A. L., and Polozov, O. Generative code modeling with graphs. In *7th International Conference on Learning Representations, ICLR 2019, New Orleans, LA, USA, May 6-9, 2019*, 2019.
- Cai, R., Yang, G., Averbuch-Elor, H., Hao, Z., Belongie, S. J., Snavely, N., and Hariharan, B. Learning gradient fields for shape generation. In *ECCV*, 2020.
- Chen, N., Zhang, Y., Zen, H., Weiss, R. J., Norouzi, M., and Chan, W. Wavegrad: Estimating gradients for waveform generation. In *ICLR*, 2021.
- Costa, F. and De Grave, K. Fast neighborhood subgraph pairwise distance kernel. In *Proceedings of the 26th International Conference on Machine Learning*, pp. 255–262. Omnipress; Madison, WI, USA, 2010.
- Dai, H., Nazi, A., Li, Y., Dai, B., and Schuurmans, D. Scalable deep generative modeling for sparse graphs. In *International Conference on Machine Learning*, pp. 2302–2312. PMLR, 2020.
- De Cao, N. and Kipf, T. Molgan: An implicit generative model for small molecular graphs. *ICML 2018 workshop on Theoretical Foundations and Applications of Deep Generative Models*, 2018.
- Dhariwal, P. and Nichol, A. Diffusion models beat gans on image synthesis. *arXiv:2105.05233*, 2021.
- Dockhorn, T., Vahdat, A., and Kreis, K. Score-based generative modeling with critically-damped langevin diffusion. *arXiv:2112.07068*, 2021.
- Grover, A., Zweig, A., and Ermon, S. Graphite: Iterative generative modeling of graphs. In *Proceedings of the 36th International Conference on Machine Learning, ICML 2019, 9-15 June 2019, Long Beach, California, USA*, volume 97 of *Proceedings of Machine Learning Research*, pp. 2434–2444. PMLR, 2019.
- Ho, J., Jain, A., and Abbeel, P. Denoising diffusion probabilistic models. In *NeurIPS*, 2020.
- Hyvärinen, A. Estimation of non-normalized statistical models by score matching. *J. Mach. Learn. Res.*, 6:695–709, 2005.
- Irwin, J. J., Sterling, T., Mysinger, M. M., Bolstad, E. S., and Coleman, R. G. Zinc: a free tool to discover chemistry for biology. *Journal of chemical information and modeling*, 52(7):1757–1768, 2012.
- Jeong, M., Kim, H., Cheon, S. J., Choi, B. J., and Kim, N. S. Diff-ts: A denoising diffusion model for text-to-speech. *arXiv:2104.01409*, 2021.
- Jin, W., Barzilay, R., and Jaakkola, T. Junction tree variational autoencoder for molecular graph generation. In *International Conference on Machine Learning*, pp. 2323–2332. PMLR, 2018.
- Jin, W., Barzilay, R., and Jaakkola, T. Hierarchical generation of molecular graphs using structural motifs. In *International Conference on Machine Learning*, pp. 4839–4848. PMLR, 2020.
- Keriven, N. and Peyré, G. Universal invariant and equivariant graph neural networks. In *Advances in Neural Information Processing Systems 32: Annual Conference on Neural Information Processing Systems 2019, NeurIPS 2019, December 8-14, 2019, Vancouver, BC, Canada*, pp. 7090–7099, 2019.
- Kong, Z., Ping, W., Huang, J., Zhao, K., and Catanzaro, B. Diffwave: A versatile diffusion model for audio synthesis. In *ICLR*, 2021.
- Landrum, G. et al. Rdkit: Open-source cheminformatics software, 2016. URL <http://www.rdkit.org/>, <https://github.com/rdkit/rdkit>, 2016.
- Lee, H., Hyung, E., and Hwang, S. J. Rapid neural architecture search by learning to generate graphs from datasets. In *9th International Conference on Learning Representations, ICLR 2021, Virtual Event, Austria, 2021*.
- Li, Y., Vinyals, O., Dyer, C., Pascanu, R., and Battaglia, P. W. Learning deep generative models of graphs. *arXiv:1803.03324*, 2018a.
- Li, Y., Zhang, L., and Liu, Z. Multi-objective de novo drug design with conditional graph generative model. *J. Cheminformatics*, 10(1):33:1–33:24, 2018b.
- Li, Y., Zhang, L., and Liu, Z. Multi-objective de novo drug design with conditional graph generative model. *J. Cheminformatics*, 10(1):33:1–33:24, 2018c.
- Liao, R., Li, Y., Song, Y., Wang, S., Hamilton, W., Duvenaud, D. K., Urtasun, R., and Zemel, R. Efficient graph generation with graph recurrent attention networks. *Advances in Neural Information Processing Systems*, 32: 4255–4265, 2019.
- Liu, J., Kumar, A., Ba, J., Kiros, J., and Swersky, K. Graph normalizing flows. In *NeurIPS*, 2019.

- Liu, M., Luo, Y., Wang, L., Xie, Y., Yuan, H., Gui, S., Yu, H., Xu, Z., Zhang, J., Liu, Y., Yan, K., Liu, H., Fu, C., Oztekin, B. M., Zhang, X., and Ji, S. DIG: A turnkey library for diving into graph deep learning research. *Journal of Machine Learning Research*, 22(240):1–9, 2021a.
- Liu, M., Yan, K., Oztekin, B., and Ji, S. Graphebm: Molecular graph generation with energy-based models. In *Energy Based Models Workshop-ICLR 2021*, 2021b.
- Luo, S. and Hu, W. Diffusion probabilistic models for 3d point cloud generation. In *CVPR*, 2021.
- Luo, Y., Yan, K., and Ji, S. Graphdf: A discrete flow model for molecular graph generation. *International Conference on Machine Learning*, 2021.
- Ma, T., Chen, J., and Xiao, C. Constrained generation of semantically valid graphs via regularizing variational autoencoders. *Advances in Neural Information Processing Systems*, 31:7113–7124, 2018.
- Madhawa, K., Ishiguro, K., Nakago, K., and Abe, M. Graph-ntp: An invertible flow model for generating molecular graphs. *arXiv preprint arXiv:1905.11600*, 2019.
- Mittal, G., Engel, J. H., Hawthorne, C., and Simon, I. Symbolic music generation with diffusion models. In *ISMIR*, 2021.
- Neal, R. Mcmc using hamiltonian dynamics. *Handbook of Markov Chain Monte Carlo*, 06 2012.
- Niu, C., Song, Y., Song, J., Zhao, S., Grover, A., and Ermon, S. Permutation invariant graph generation via score-based generative modeling. In *AISTATS*, 2020.
- O’Bray, L., Horn, M., Rieck, B., and Borgwardt, K. M. Evaluation metrics for graph generative models: Problems, pitfalls, and practical solutions. *arXiv:2106.01098*, 2021.
- Parisi, G. Correlation functions and computer simulations. *Nuclear Physics B*, 180(3):378–384, 1981.
- Paszke, A., Gross, S., Massa, F., Lerer, A., Bradbury, J., Chanan, G., Killeen, T., Lin, Z., Gimelshein, N., Antiga, L., Desmaison, A., Kopf, A., Yang, E., DeVito, Z., Raison, M., Tejani, A., Chilamkurthy, S., Steiner, B., Fang, L., Bai, J., and Chintala, S. Pytorch: An imperative style, high-performance deep learning library. In *Advances in Neural Information Processing Systems* 32, pp. 8024–8035. Curran Associates, Inc., 2019.
- Popova, M., Shvets, M., Oliva, J., and Isayev, O. Molecular-rnn: Generating realistic molecular graphs with optimized properties. *arXiv preprint arXiv:1905.13372*, 2019.
- Preuer, K., Renz, P., Unterthiner, T., Hochreiter, S., and Klambauer, G. Fréchet chemnet distance: a metric for generative models for molecules in drug discovery. *Journal of chemical information and modeling*, 58(9):1736–1741, 2018.
- Ramakrishnan, R., Dral, P. O., Rupp, M., and Von Lilienfeld, O. A. Quantum chemistry structures and properties of 134 kilo molecules. *Scientific data*, 1(1):1–7, 2014.
- Schomburg, I., Chang, A., Ebeling, C., Gremse, M., Heldt, C., Huhn, G., and Schomburg, D. Brenda, the enzyme database: updates and major new developments. *Nucleic Acids Res.*, 32(Database-Issue):431–433, 2004.
- Sen, P., Namata, G. M., Bilgic, M., Getoor, L., Gallagher, B., and Eliassi-Rad, T. Collective classification in network data. *AI Magazine*, 29(3):93–106, 2008.
- Shi, C., Xu, M., Zhu, Z., Zhang, W., Zhang, M., and Tang, J. Graphaf: a flow-based autoregressive model for molecular graph generation. In *International Conference on Learning Representations*, 2020.
- Simonovsky, M. and Komodakis, N. Graphvae: Towards generation of small graphs using variational autoencoders. In *ICANN*, 2018.
- Song, J., Meng, C., and Ermon, S. Denoising diffusion implicit models. In *ICLR*, 2021a.
- Song, Y. and Ermon, S. Generative modeling by estimating gradients of the data distribution. In *NeurIPS*, 2019.
- Song, Y. and Ermon, S. Improved techniques for training score-based generative models. In *NeurIPS*, 2020.
- Song, Y., Sohl-Dickstein, J., Kingma, D. P., Kumar, A., Ermon, S., and Poole, B. Score-based generative modeling through stochastic differential equations. In *ICLR*, 2021b.
- Strang, G. On the construction and comparison of difference schemes. *SIAM Journal on Numerical Analysis*, 5:506–517, 1968.
- Särkkä, S. and Solin, A. *Applied Stochastic Differential Equations*. Institute of Mathematical Statistics Textbooks. Cambridge University Press, 2019.
- Trotter, H. F. On the product of semi-groups of operators. In *Proceedings of the American Mathematical Society*, 1959.
- Vahdat, A., Kreis, K., and Kautz, J. Score-based generative modeling in latent space. *arXiv:2106.05931*, 2021.
- Wang, H., Wang, J., Wang, J., Zhao, M., Zhang, W., Zhang, F., Xie, X., and Guo, M. Graphgan: Graph representation learning with generative adversarial nets. In *AAAI*, 2018.

- Xie, S., Kirillov, A., Girshick, R. B., and He, K. Exploring randomly wired neural networks for image recognition. In *2019 IEEE/CVF International Conference on Computer Vision, ICCV 2019, Seoul, Korea (South), October 27 - November 2, 2019*, pp. 1284–1293. IEEE, 2019.
- You, J., Liu, B., Ying, R., Pande, V., and Leskovec, J. Graph convolutional policy network for goal-directed molecular graph generation. In *Proceedings of the 32nd International Conference on Neural Information Processing Systems*, pp. 6412–6422, 2018a.
- You, J., Ying, R., Ren, X., Hamilton, W., and Leskovec, J. Graphrnn: Generating realistic graphs with deep autoregressive models. In *International conference on machine learning*, pp. 5708–5717. PMLR, 2018b.
- Zang, C. and Wang, F. Moflow: an invertible flow model for generating molecular graphs. In *Proceedings of the 26th ACM SIGKDD International Conference on Knowledge Discovery & Data Mining*, pp. 617–626, 2020.

Appendix

A. Derivations

A.1. Deriving the Denoising Score Matching Objectives

The original score matching objective can be written as follows:

$$\mathbb{E}_{\mathbf{G}_t} \left\| \mathbf{s}_\theta(\mathbf{G}_t, t) - \nabla_{\mathbf{X}_t} \log p_t(\mathbf{G}_t) \right\|_2^2 = \mathbb{E}_{\mathbf{G}_t} \left\| \mathbf{s}_\theta(\mathbf{G}_t, t) \right\|_2^2 - \mathbb{E}_{\mathbf{G}_t} \left\langle \mathbf{s}_\theta, \nabla_{\mathbf{X}_t} \log p_t(\mathbf{G}_t) \right\rangle + C_1, \quad (12)$$

where C_1 is a constant that does not depend on θ . Further, the denoising score matching objective can be written as follows:

$$\begin{aligned} \mathbb{E}_{\mathbf{G}_0} \mathbb{E}_{\mathbf{G}_t | \mathbf{G}_0} \left\| \mathbf{s}_\theta(\mathbf{G}_t, t) - \nabla_{\mathbf{X}_t} \log p_t(\mathbf{G}_t | \mathbf{G}_0) \right\|_2^2 &= \mathbb{E}_{\mathbf{G}_0} \mathbb{E}_{\mathbf{G}_t | \mathbf{G}_0} \left\| \mathbf{s}_\theta(\mathbf{G}_t, t) \right\|_2^2 \\ &\quad - \mathbb{E}_{\mathbf{G}_0} \mathbb{E}_{\mathbf{G}_t | \mathbf{G}_0} \left\langle \mathbf{s}_\theta, \nabla_{\mathbf{X}_t} \log p_t(\mathbf{G}_t | \mathbf{G}_0) \right\rangle + C_2, \end{aligned} \quad (13)$$

where C_2 is also a constant that does not depend on θ . From the following equivalence,

$$\begin{aligned} \mathbb{E}_{\mathbf{G}_t} \left\langle \mathbf{s}_\theta, \nabla_{\mathbf{X}_t} \log p_t(\mathbf{G}_t) \right\rangle &= \int_{\mathbf{G}_t} p(\mathbf{G}_t) \left\langle \mathbf{s}_\theta, \nabla_{\mathbf{X}_t} \log p_t(\mathbf{G}_t) \right\rangle d\mathbf{G}_t \\ &= \int_{\mathbf{G}_t} \left\langle \mathbf{s}_\theta, \nabla_{\mathbf{X}_t} p_t(\mathbf{G}_t) \right\rangle d\mathbf{G}_t \\ &= \int_{\mathbf{G}_t} \left\langle \mathbf{s}_\theta, \nabla_{\mathbf{X}_t} \int_{\mathbf{G}_0} p(\mathbf{G}_0) p_t(\mathbf{G}_t | \mathbf{G}_0) d\mathbf{G}_0 \right\rangle d\mathbf{G}_t \\ &= \int_{\mathbf{G}_t} \left\langle \mathbf{s}_\theta, \nabla_{\mathbf{X}_t} \int_{\mathbf{G}_0} p(\mathbf{G}_0) p_t(\mathbf{G}_t | \mathbf{G}_0) d\mathbf{G}_0 \right\rangle d\mathbf{G}_t \\ &= \int_{\mathbf{G}_t} \left\langle \mathbf{s}_\theta, \int_{\mathbf{G}_0} p(\mathbf{G}_0) \nabla_{\mathbf{X}_t} p_t(\mathbf{G}_t | \mathbf{G}_0) d\mathbf{G}_0 \right\rangle d\mathbf{G}_t \\ &= \int_{\mathbf{G}_t} \int_{\mathbf{G}_0} p(\mathbf{G}_0) p_t(\mathbf{G}_t | \mathbf{G}_0) \left\langle \mathbf{s}_\theta, \nabla_{\mathbf{X}_t} \log p_t(\mathbf{G}_t | \mathbf{G}_0) \right\rangle d\mathbf{G}_0 d\mathbf{G}_t \\ &= \mathbb{E}_{\mathbf{G}_0} \mathbb{E}_{\mathbf{G}_t | \mathbf{G}_0} \left\langle \mathbf{s}_\theta, \nabla_{\mathbf{X}_t} \log p_t(\mathbf{G}_t | \mathbf{G}_0) \right\rangle, \end{aligned}$$

we can conclude that the two objectives are equivalent:

$$\mathbb{E}_{\mathbf{G}_0} \mathbb{E}_{\mathbf{G}_t | \mathbf{G}_0} \left\| \mathbf{s}_\theta(\mathbf{G}_t, t) - \nabla_{\mathbf{X}_t} \log p_t(\mathbf{G}_t | \mathbf{G}_0) \right\|_2^2 = \mathbb{E}_{\mathbf{G}_t} \left\| \mathbf{s}_\theta(\mathbf{G}_t, t) - \nabla_{\mathbf{X}_t} \log p_t(\mathbf{G}_t) \right\|_2^2 + C_2 - C_1. \quad (14)$$

Similarly, computing the gradient with respect to \mathbf{A}_t , we can show that the following two objectives are also equivalent:

$$\mathbb{E}_{\mathbf{G}_0} \mathbb{E}_{\mathbf{G}_t | \mathbf{G}_0} \left\| \mathbf{s}_\phi(\mathbf{G}_t, t) - \nabla_{\mathbf{A}_t} \log p_t(\mathbf{G}_t | \mathbf{G}_0) \right\|_2^2 = \mathbb{E}_{\mathbf{G}_t} \left\| \mathbf{s}_\phi(\mathbf{G}_t, t) - \nabla_{\mathbf{A}_t} \log p_t(\mathbf{G}_t) \right\|_2^2 + C_4 - C_3, \quad (15)$$

where C_3 and C_4 are constants that does not depend on ϕ .

A.2. Deriving New Objectives for GDSS

It is enough to show that $\nabla_{\mathbf{X}_t} \log p_{0t}(\mathbf{G}_t | \mathbf{G}_0)$ is equal to $\nabla_{\mathbf{X}_t} \log p_{0t}(\mathbf{X}_t | \mathbf{X}_0)$. Using the chain rule,

$$\frac{\partial \log p_{0t}(\mathbf{A}_t | \mathbf{A}_0)}{\partial (\mathbf{X}_t)_{ij}} = \text{Tr} \left[\nabla_{\mathbf{A}_t} \log p_{0t}(\mathbf{A}_t | \mathbf{A}_0) \underbrace{\frac{\partial \mathbf{A}_t}{\partial (\mathbf{X}_t)_{ij}}}_{=0} \right] = 0, \quad (16)$$

we can derive that $\nabla_{\mathbf{X}_t} \log p_{0t}(\mathbf{A}_t | \mathbf{A}_0) = 0$. Therefore,

$$\nabla_{\mathbf{X}_t} \log p_{0t}(\mathbf{G}_t | \mathbf{G}_0) = \nabla_{\mathbf{X}_t} \log p_{0t}(\mathbf{X}_t | \mathbf{X}_0) + \underbrace{\nabla_{\mathbf{X}_t} \log p_{0t}(\mathbf{A}_t | \mathbf{A}_0)}_{=0} = \nabla_{\mathbf{X}_t} \log p_{0t}(\mathbf{X}_t | \mathbf{X}_0). \quad (17)$$

Similarly, computing the gradient with respect to \mathbf{A}_t , we can also show that $\nabla_{\mathbf{A}_t} \log p_{0t}(\mathbf{G}_t | \mathbf{G}_0)$ is equal to $\nabla_{\mathbf{A}_t} \log p_{0t}(\mathbf{A}_t | \mathbf{A}_0)$.

A.3. Action of the Fokker-Planck Operators

The Fokker-Planck operator $\hat{\mathcal{L}}_F^*$ corresponds to the diffusion process described by the F term in Eq. (10):

$$\begin{cases} d\mathbf{X}_t = \mathbf{f}_{1,t}(\mathbf{X}_t)d\bar{t} + g_{1,t}d\bar{\mathbf{w}}_1 \\ d\mathbf{A}_t = \mathbf{f}_{2,t}(\mathbf{A}_t)d\bar{t} + g_{2,t}d\bar{\mathbf{w}}_2 \end{cases}, \quad (18)$$

Since the SDEs in Eq. (18) have affine drift and diffusion coefficients, the evolution of \mathbf{X}_t and \mathbf{A}_t is analytically tractable. Notice that the diffusion process described by Eq. (18) is same as the forward diffusion process of Eq. (1), with slight difference of an infinitesimal negative time step $d\bar{t}$ instead of a positive time step dt . Therefore, the action of $e^{\frac{\delta t}{2}\hat{\mathcal{L}}_F^*}$ can be represented by the transition kernel of the forward diffusion process $p_{st}(\cdot|\cdot)$ as follows:

$$e^{\frac{\delta t}{2}\hat{\mathcal{L}}_F^*}\mathbf{G}_t \sim p_{t,t-\delta t/2}(\mathbf{G}_{t-\delta t/2}|\mathbf{G}_t). \quad (19)$$

We provide the explicit form of the transition kernel in Section A.4 of Appendix. Further, Fokker-Planck operator $\hat{\mathcal{L}}_S^*$ corresponds to the evolution of \mathbf{X}_t and \mathbf{A}_t described by the S terms in Eq. (10):

$$\begin{cases} \mathbf{X}_t = -g_{1,t}^2\mathbf{s}_{\theta,t}(\mathbf{X}_t, \mathbf{A}_t)d\bar{t} \\ \mathbf{A}_t = -g_{2,t}^2\mathbf{s}_{\phi,t}(\mathbf{X}_t, \mathbf{A}_t)d\bar{t} \end{cases}, \quad (20)$$

which is a system of ODEs with infinitesimal negative time step $d\bar{t}$. Hence, the action of $e^{\delta t\hat{\mathcal{L}}_S^*}$ can be approximated with the simple Euler step for a positive time step δt :

$$\begin{aligned} e^{\delta t\hat{\mathcal{L}}_S^*}\mathbf{X}_t &\approx \mathbf{X}_t + g_{1,t}^2\mathbf{s}_{\theta,t}(\mathbf{X}_t, \mathbf{A}_t)\delta t, \\ e^{\delta t\hat{\mathcal{L}}_S^*}\mathbf{A}_t &\approx \mathbf{A}_t + g_{2,t}^2\mathbf{s}_{\phi,t}(\mathbf{X}_t, \mathbf{A}_t)\delta t, \end{aligned} \quad (21)$$

which we refer to this approximated action as $e^{\delta t\mathcal{L}_S^{Euler}}$. From the action of $e^{\frac{\delta t}{2}\hat{\mathcal{L}}_F^*}$ and $e^{\delta t\hat{\mathcal{L}}_S^*}$ with the Trotter theorem (Trotter, 1959), we can approximate the intractable solution $e^{t(\hat{\mathcal{L}}_F^*+\hat{\mathcal{L}}_S^*)}$ as follows (Dockhorn et al., 2021):

$$\begin{aligned} e^{t(\hat{\mathcal{L}}_F^*+\hat{\mathcal{L}}_S^*)} &\approx \left[e^{\frac{\delta t}{2}\hat{\mathcal{L}}_F^*} e^{\delta t\hat{\mathcal{L}}_S^*} e^{\frac{\delta t}{2}\hat{\mathcal{L}}_F^*} \right]^M + O(M\delta t^3) \\ &= \left[e^{\frac{\delta t}{2}\hat{\mathcal{L}}_F^*} e^{\delta t\mathcal{L}_S^{Euler}} e^{\frac{\delta t}{2}\hat{\mathcal{L}}_F^*} \right]^M + MO(\delta t^2) \end{aligned} \quad (22)$$

$$= \left[e^{\frac{\delta t}{2}\hat{\mathcal{L}}_F^*} e^{\delta t\mathcal{L}_S^{Euler}} e^{\frac{\delta t}{2}\hat{\mathcal{L}}_F^*} \right]^M + O(\delta t), \quad (23)$$

for sufficiently large number of steps M and a time step $\delta t = t/M$. From Eq. (22) and Eq. (23), we can see that the prediction step of S4 has local error $\mathcal{O}(\delta t^2)$ and global error $\mathcal{O}(\delta t)$.

A.4. Derivation of the Transition Kernel

We provide an explicit form of the transition kernel for two types of SDE, namely VPSDE and VESDE (Song et al., 2021b). We consider the transition kernel from time t to $t - \delta t$ for sufficiently small time step δt with \mathbf{x}_t given, considering the input as discrete state corresponding to normal distribution with 0 variance.

VPSDE The VPSDE has the form of:

$$d\mathbf{x} = -\frac{1}{2}\beta_t\mathbf{x}dt + \sqrt{\beta_t}d\mathbf{w}, \quad (24)$$

where $\beta_t = \beta_{min} + t(\beta_{max} - \beta_{min})$ for $t \in [0, 1]$. Using the result of Eq.(5.50) and (5.51) of Särkkä & Solin (2019), we can obtain the following:

$$p_{t,t-\delta t}(\mathbf{x}_{t-\delta t}|\mathbf{x}_t) = \mathcal{N}(\mathbf{x}_{t-\delta t} | \mu_t\mathbf{x}_t, \Sigma_t), \quad (25)$$

where $\mu_t = e^{C_t}$ and $\Sigma_t = \mathbf{I} - \mathbf{I}e^{-2C_t}$ for

$$C_t = \frac{1}{2} \int_{t-\delta t}^t \beta_s ds = \frac{\delta t}{4} \left(2\beta_{min} + (2t + \delta t)(\beta_{max} - \beta_{min}) \right). \quad (26)$$

VESDE The VESDE has the form of:

$$d\mathbf{x} = \sigma_{min} \left(\frac{\sigma_{max}}{\sigma_{min}} \right)^t \sqrt{2 \log \frac{\sigma_{max}}{\sigma_{min}}} d\mathbf{w} \quad (27)$$

for $t \in (0, 1]$. Using the result of Eq.(5.50) and (5.51) of [Särkkä & Solin \(2019\)](#), we can obtain the following:

$$p_{t,t-\delta t}(\mathbf{x}_{t-\delta t} | \mathbf{x}_t) = \mathcal{N}(\mathbf{x}_{t-\delta t} | \mathbf{x}_t, \Sigma_t), \quad (28)$$

where $\Sigma_t = \Sigma_t \mathbf{I}$ is given as:

$$\Sigma_t = \sigma_{min}^2 \left(\frac{\sigma_{max}}{\sigma_{min}} \right)^{2t} - \sigma_{min}^2 \left(\frac{\sigma_{max}}{\sigma_{min}} \right)^{2t-2\delta t}. \quad (29)$$

A.5. Symmetric Splitting for the System of SDEs

We provide the pseudo-code for the proposed S4 solver in [Algorithm 1](#).

Algorithm 1 Symmetric Splitting for the System of SDEs (S4)

Input: Score models $s_{\theta,t}$ and $s_{\phi,t}$, number of sampling steps M , step size δt , transition kernels $p_{st}(\cdot|\cdot)$ of the forward diffusion in Eq. (1), Langevin MCMC step size α , scaling coefficient ϵ_s

Output: $\mathbf{X}_0, \mathbf{A}_0$: the solution to Eq. (10)

```

1:  $t = T$ 
2: Sample from the prior distribution  $\mathbf{X}_M, \mathbf{A}_M \sim p_T$ 
3: for  $m = M - 1$  to 0 do
4:    $\mathbf{S}_X \leftarrow s_{\theta,t}(\mathbf{X}_{m+1}, \mathbf{A}_{m+1}); \mathbf{S}_A \leftarrow s_{\phi,t}(\mathbf{X}_{m+1}, \mathbf{A}_{m+1})$  ▷ score computation step
5:    $\tilde{\mathbf{X}}_{m+1} \leftarrow \mathbf{X}_{m+1} + \frac{\alpha}{2} \mathbf{S}_X + \epsilon_s \sqrt{\alpha} \mathbf{z}_X; \mathbf{z}_X \sim \mathcal{N}(\mathbf{0}, \mathbf{I}_X)$ 
6:    $\tilde{\mathbf{A}}_{m+1} \leftarrow \mathbf{A}_{m+1} + \frac{\alpha}{2} \mathbf{S}_A + \epsilon_s \sqrt{\alpha} \mathbf{z}_A; \mathbf{z}_A \sim \mathcal{N}(\mathbf{0}, \mathbf{I}_A)$  ▷ correction step
7:    $t' \leftarrow t - \delta t/2$ 
8:    $\tilde{\mathbf{X}}_m \sim p_{t,t'}(\tilde{\mathbf{X}}_m | \mathbf{X}_{m+1}); \tilde{\mathbf{A}}_m \sim p_{t,t'}(\tilde{\mathbf{A}}_m | \mathbf{A}_{m+1})$ 
9:    $\tilde{\mathbf{X}}_m \leftarrow \tilde{\mathbf{X}}_m + g_{1,t}^2 \mathbf{S}_X \delta t; \tilde{\mathbf{A}}_m \leftarrow \tilde{\mathbf{A}}_m + g_{2,t}^2 \mathbf{S}_A \delta t$ 
10:   $t \leftarrow t - \delta t$ 
11:   $\mathbf{X}_m \sim p_{t',t}(\mathbf{X}_m | \tilde{\mathbf{X}}_m); \mathbf{A}_m \sim p_{t',t}(\mathbf{A}_m | \tilde{\mathbf{A}}_m)$  ▷ prediction step
12: end for
13: Return:  $\mathbf{X}_0, \mathbf{A}_0$ 
    
```

B. Details for Score-based Graph Generation

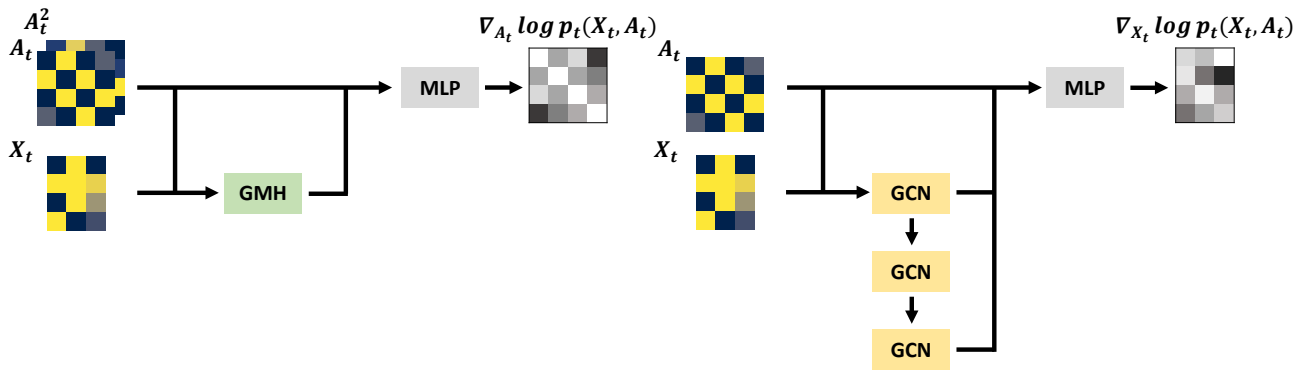


Figure 5: **The architecture of the score-based models of GDSS.** (Left) The score-based model s_{ϕ} estimating $\nabla_{A_t} \log p_t(\mathbf{X}_t, \mathbf{A}_t)$ is composed of GMH blocks and MLP layers. (Right) The score-based model s_{θ} estimating $\nabla_{X_t} \log p_t(\mathbf{X}_t, \mathbf{A}_t)$ is composed of GCN layers and MLP layers. Both models take \mathbf{X}_t and \mathbf{A}_t as input and estimate the partial scores with respect to \mathbf{A}_t and \mathbf{X}_t , respectively.

B.1. Score-based Model Architecture

We illustrate the architecture of the proposed score models s_{θ} and s_{ϕ} described in [Section 3.2](#), in [Figure 5](#).

B.2. Generating Samples from the Reverse Diffusion Process

We first sample N , the number of nodes to be generated from the empirical distribution of the number of nodes in the training dataset as done in Li et al. (2018b) and Niu et al. (2020). Then we sample noise \mathbf{X}_T of size $N \times F$ and \mathbf{A}_T of size $N \times N$ from the prior distribution, and simulate the reverse-time system of SDEs in Eq. (10) to obtain the solution \mathbf{X}_0 and \mathbf{A}_0 . Lastly, we quantize \mathbf{A}_0 with the operation $1_{x>0.5}$ to obtain the 0-1 adjacency matrix.

C. Experimental Details

C.1. Hyperparameters of GDSS

We provide the hyperparameters used in the experiments in Table 3.

Table 3: Hyperparameters of GDSS used in the experiments.

	Hyperparameter	Ego-small	Community-small	Enzymes	Grid	QM9	ZINC250k
s_θ	Number of GCN layers	2	3	5	5	2	2
	Hidden dimension	32	32	32	7	16	16
s_ϕ	Number of attention heads	4	4	4	4	4	4
	Number of initial channels	2	2	2	2	2	2
	Number of hidden channels	8	8	8	8	8	8
	Number of final channels	4	4	4	4	4	4
	Number of GCN layers	5	5	7	7	3	6
	Hidden dimension	32	32	32	32	16	16
SDE for \mathbf{X}	Type	VP	VP	VP	VP	VE	VP
	Number of sampling steps	1000	1000	1000	1000	1000	1000
	β_{min}	0.1	0.1	0.1	0.1	0.1	0.1
	β_{max}	1.0	1.0	1.0	1.0	1.0	1.0
SDE for \mathbf{A}	Type	VP	VP	VE	VE	VE	VE
	Number of sampling steps	1000	1000	1000	1000	1000	1000
	β_{min}	0.1	0.1	0.2	0.2	0.1	0.1
	β_{max}	1.0	1.0	1.0	0.8	1.0	1.0
Solver	Type	EM	EM + Langevin	S4	Rev. + Langevin	Rev. + Langevin	Rev. + Langevin
	SNR	0.05	0.05	0.15	0.1	0.2	0.2
	Scale coefficient	0.4	0.7	0.7	0.7	0.7	0.9
Train	Optimizer	Adam	Adam	Adam	Adam	Adam	Adam
	Learning rate	1×10^{-2}	1×10^{-2}	1×10^{-2}	1×10^{-2}	5×10^{-3}	5×10^{-3}
	Weight decay	1×10^{-4}					
	Batch size	128	128	64	8	1024	1024
	Number of epochs	5000	5000	5000	5000	300	500
	EMA	-	-	0.999	0.999	-	-

C.2. Toy Experiment

In this subsection, we provide the details for the toy experiment presented in Section 3.1. We construct the distribution of the data with bivariate Gaussian mixture of the form:

$$p_{data}(\mathbf{x}) = \mathcal{N}(\mathbf{x} \mid \mu_1, \Sigma_1) + \mathcal{N}(\mathbf{x} \mid \mu_2, \Sigma_2), \quad (30)$$

where the mean and variance are given as follows:

$$\mu_1 = \begin{pmatrix} 0.5 \\ 0.5 \end{pmatrix}, \quad \mu_2 = \begin{pmatrix} -0.5 \\ -0.5 \end{pmatrix}$$

$$\Sigma_1 = \Sigma_2 = 0.1^2 \begin{pmatrix} 1.0 & 0.9 \\ 0.9 & 1.0 \end{pmatrix}.$$

For each diffusion method, namely GDSS, GDSS-seq, and independent, we train two models, each estimating the partial scores or scores with respect to each variable. We fix the number of CNN layers in the model to 20 with residual paths and set the hidden dimension as 512. We further use VPSDE for the diffusion process of each variable with $\beta_{min} = 0.01$ and

$\beta_{max} = 0.05$. We train the models for 5000 epochs with batch size 2048 sampled from the data distribution. We generate 2^{13} samples for each diffusion method, shown in Figure 2.

C.3. Generic Graph Generation

The information about the graph datasets, namely Ego-small, Community-small, Enzymes and Grid, are explained in Section 4.1 and Table 1.

Implementation Details For a fair evaluation of the generic graph generation task, we follow the standard setting of existing works (You et al., 2018b; Liu et al., 2019; Niu et al., 2020) from the node features to the data splitting. Especially, for Ego-small and Community-small datasets, we report the means of 15 runs, 3 different runs for 5 independently trained models. For Enzymes and Grid dataset, since the baselines including GraphVAE and EDP-GNN take more than 3 days for single training, we report the means of 3 different runs. For the baselines, we use the hyperparameters given by the original work, and further search for the best performance if none exists.

For GDSS, we initialize the node features as the one-hot encoding of degrees. We perform the grid search to choose the best signal-to-noise ratio (SNR) $\in \{0.05, 0.1, 0.15, 0.2\}$ and scale coefficient $\in \{0.1, 0.2, 0.3, 0.4, 0.5, 0.6, 0.7, 0.8, 0.9, 1.0\}$. We select the best MMD with the lowest average of three graph statistics, degree, clustering coefficient, and orbit. Further, we observed that applying exponential moving average (EMA) Song & Ermon (2020) for large graph dataset, Enzymes and Grid, improves the performance and lowers the variance. We report the hyperparameters used in the experiment in Table 3.

C.4. Molecule Generation

The information about the QM9 and ZINC250k datasets is summarized in Table 4.

Table 4: Information of the molecular datasets.

Dataset	Number of graphs	Number of nodes	Number of node types	Number of edge types
QM9	133,885	$1 \leq V \leq 9$	4	3
ZINC250k	249,455	$6 \leq V \leq 38$	9	3

Implementation Details of GDSS and GDSS-seq Each molecule is preprocessed into a graph of $X \in \{0, 1\}^{N \times F}$ and $A \in \{0, 1, 2, 3\}^{N \times N}$, where N is the maximum number of atoms in a molecule of the dataset, and F is the number of possible atom types. The entries of A indicate single, double, or triple bonds. Following the standard procedure, the molecules are kekulized by the RDKit library (Landrum et al., 2016) and hydrogen atoms are removed. We make use of the valency correction proposed by Zang & Wang (2020).

We perform the grid search to choose the best signal-to-noise ratio (SNR) $\in \{0.1, 0.2\}$ and scale coefficient $\in \{0.1, 0.2, 0.3, 0.4, 0.5, 0.6, 0.7, 0.8, 0.9, 1.0\}$. Since the low novelty value leads to low FCD and NSPDK MMD values even though it is undesirable and meaningless, we choose the hyperparameters that exhibit the best FCD value among those show novelty that exceeds 85%. After sampling through the reverse diffusion process, we quantize the entries of the adjacency matrices to $\{0, 1, 2, 3\}$ by clipping the values of $(-\infty, 0.5)$ to 0, the values of $[0.5, 1.5)$ to 1, the values of $[1.5, 2.5)$ to 2, and the values of $[2.5, +\infty)$ to 3. We report the hyperparameters used in the experiment in Table 3.

Implementation Details of Baselines We utilize the DIG (Liu et al., 2021a) library to generate molecules with GraphDF and GraphEBM. To experiment with GraphAF, we use the DIG library for the QM9 dataset, and use the official code² for the ZINC250k dataset. We use the official code³ for MoFlow. We follow the experimental setting reported in the respective original papers and the codes for these models. For EDP-GNN, we use the same preprocessing and postprocessing procedures as in GDSS and GDSS-seq, except we divide the adjacency matrices by 3 to ensure the entries are in the range of $[0, 1]$ before feeding them into the model. We conduct the grid search to choose the best size of the Langevin step $\in \{0.01, 0.005, 0.001\}$ and noise scale $\in \{0.1, 0.2, 0.3, 0.4, 0.5, 0.6, 0.7, 0.8, 0.9, 1.0\}$, and apply the same tuning criterion as in GDSS and GDSS-seq.

²<https://github.com/DeepGraphLearning/GraphAF>

³<https://github.com/calvin-zcx/moflow>

C.5. Computing Resources

For all experiments, we utilize PyTorch (Paszke et al., 2019) to implement GDSS and train the score models on TITAN XP, TITAN RTX, GeForce RTX 2080 Ti, GeForce RTX 3090, or RTX A5000 GPU.

D. Additional Experimental Results

D.1. Generic Graph Generation

We additionally report the standard deviation of the generation results of Table 1 in Table 5 and Table 6.

Table 5: **Generation results of GDSS on the Ego-small and the Community-small datasets.** We report the MMD distance between the test datasets and generated graphs with the standard deviation.

	Ego-small			Community-small		
	Real, $4 \leq V \leq 18$			Synthetic, $12 \leq V \leq 20$		
	Deg.	Clus.	Orbit	Deg.	Clus.	Orbit
GDSS-seq (Ours)	0.032 ± 0.006	0.027 ± 0.005	0.011 ± 0.007	0.090 ± 0.021	0.123 ± 0.200	0.007 ± 0.003
GDSS (Ours)	0.021 ± 0.008	0.024 ± 0.007	0.007 ± 0.005	0.045 ± 0.028	0.086 ± 0.022	0.007 ± 0.004

Table 6: **Generation results on the Enzymes and the Grid datasets.** We report the MMD distance between the test datasets and generated graphs with the standard deviation. Best results are highlighted in bold, and for all MMD metrics, the smaller the better. Hyphen (-) denotes out-of-resources that take more than 10 days or not applicable due to memory issue. * denotes our own implementation and † indicates unreproducible results.

	Enzymes			Grid		
	Real, $10 \leq V \leq 125$			Synthetic, $100 \leq V \leq 400$		
	Deg.	Clus.	Orbit	Deg.	Clus.	Orbit
DeepGMG	-	-	-	-	-	-
GraphRNN	0.017 ± 0.007	0.062 ± 0.020	0.046 ± 0.031	0.064 ± 0.017	0.043 ± 0.022	0.021 ± 0.007
GraphAF*	1.669 ± 0.024	1.283 ± 0.019	0.266 ± 0.007	-	-	-
GraphDF*	1.503 ± 0.011	1.061 ± 0.011	0.202 ± 0.002	-	-	-
GraphVAE*	1.369 ± 0.020	0.629 ± 0.005	0.191 ± 0.020	1.619 ± 0.007	0.0 ± 0.000	0.919 ± 0.002
GNF†	-	-	-	-	-	-
EDP-GNN	0.023 ± 0.012	0.268 ± 0.164	0.082 ± 0.078	0.455 ± 0.319	0.238 ± 0.380	0.328 ± 0.278
GDSS-seq (Ours)	0.099 ± 0.083	0.225 ± 0.051	0.010 ± 0.007	0.171 ± 0.134	0.011 ± 0.001	0.223 ± 0.070
GDSS (Ours)	0.026 ± 0.008	0.061 ± 0.010	0.009 ± 0.005	0.111 ± 0.012	0.005 ± 0.000	0.070 ± 0.044

D.2. Molecule Generation

We additionally report the validity, uniqueness, and novelty of the generated molecules as well as the standard deviation of the results in Table 7 and Table 8. **Validity** is the fraction of the generated molecules that do not violate the chemical valency rule. **Uniqueness** is the fraction of the valid molecules that are unique. **Novelty** is the fraction of the valid molecules that are not included in the training set. The inference time of each model is measured on 1 TITAN RTX GPU and 20 CPU cores.

Table 7: **Generation results on the QM9 dataset.** Results are the means and the standard deviations of 3 runs. Values denoted by * are taken from the respective original papers. Other results are obtained by running open-source codes. Best results are highlighted in bold.

	Method	Validity w/o correction (%) \uparrow	NSPDK MMD \downarrow	FCD \downarrow	Validity (%) \uparrow	Uniqueness (%) \uparrow	Novelty (%) \uparrow
Autoreg.	GraphAF (Shi et al., 2020)	67*	0.020 \pm 0.003	5.268 \pm 0.403	100.00*	94.51*	88.83*
	GraphAF+FC	74.43 \pm 2.55	0.021 \pm 0.003	5.625 \pm 0.259	100.00 \pm 0.00	88.64 \pm 2.37	86.59 \pm 1.95
	GraphDF (Luo et al., 2021)	82.67*	0.063 \pm 0.001	10.816 \pm 0.020	100.00*	97.62*	98.10*
	GraphDF+FC	93.88 \pm 4.76	0.064 \pm 0.000	10.928 \pm 0.038	100.00 \pm 0.00	98.58 \pm 0.25	98.54 \pm 0.48
One-shot	MoFlow (Zang & Wang, 2020)	91.36 \pm 1.23	0.017 \pm 0.003	4.467 \pm 0.595	100.00 \pm 0.00	98.65 \pm 0.57	94.72 \pm 0.77
	EDP-GNN (Niu et al., 2020)	47.52 \pm 3.60	0.005 \pm 0.001	2.680 \pm 0.221	100.00 \pm 0.00	99.25 \pm 0.05	86.58 \pm 1.85
	GraphEBM (Liu et al., 2021b)	8.22 \pm 2.24	0.030 \pm 0.004	6.143 \pm 0.411	100.00 \pm 0.00*	97.90 \pm 0.14*	97.01 \pm 0.17*
	GDSS-seq (Ours)	94.47 \pm 1.03	0.010 \pm 0.001	4.004 \pm 0.166	100.00 \pm 0.00	94.62 \pm 1.40	85.48 \pm 1.01
	GDSS (Ours)	95.72 \pm 1.94	0.003 \pm 0.000	2.900 \pm 0.282	100.00 \pm 0.00	98.46 \pm 0.61	86.27 \pm 2.29

Table 8: **Generation results on the ZINC250k dataset.** Results are the means and the standard deviations of 3 runs. Values denoted by * are taken from the respective original papers. Other results are obtained by running open-source codes. Best results are marked as bold.

	Method	Validity w/o correction (%) \uparrow	NSPDK MMD \downarrow	FCD \downarrow	Validity (%) \uparrow	Uniqueness (%) \uparrow	Novelty (%) \uparrow
Autoreg.	GraphAF (Shi et al., 2020)	68*	0.044 \pm 0.006	16.289 \pm 0.482	100.00*	99.10*	100.00*
	GraphAF+FC	68.47 \pm 0.99	0.044 \pm 0.005	16.023 \pm 0.451	100.00 \pm 0.00	98.64 \pm 0.69	99.99 \pm 0.01
	GraphDF (Luo et al., 2021)	89.03*	0.176 \pm 0.001	34.202 \pm 0.160	100.00*	99.16*	100.00*
	GraphDF+FC	90.61 \pm 4.30	0.177 \pm 0.001	33.546 \pm 0.150	100.00 \pm 0.00	99.63 \pm 0.01	100.00 \pm 0.00
One-shot	MoFlow (Zang & Wang, 2020)	63.11 \pm 5.17	0.046 \pm 0.002	20.931 \pm 0.184	100.00 \pm 0.00	99.99 \pm 0.01	100.00 \pm 0.00
	EDP-GNN (Niu et al., 2020)	82.97 \pm 2.73	0.049 \pm 0.006	16.737 \pm 1.300	100.00 \pm 0.00	99.79 \pm 0.08	100.00 \pm 0.00
	GraphEBM (Liu et al., 2021b)	5.29 \pm 3.83	0.212 \pm 0.075	35.471 \pm 5.331	99.96 \pm 0.02*	98.79 \pm 0.15*	100.00 \pm 0.00*
	GDSS-seq (Ours)	92.39 \pm 2.72	0.030 \pm 0.003	16.847 \pm 0.097	100.00 \pm 0.00	99.94 \pm 0.02	100.00 \pm 0.00
	GDSS (Ours)	97.01 \pm 0.77	0.019 \pm 0.001	14.656 \pm 0.680	100.00 \pm 0.00	99.64 \pm 0.13	100.00 \pm 0.00

E. Visualization

E.1. Generic Graph Generation

We visualize the graphs from the training datasets and the generated graphs of each model in Figure 6.

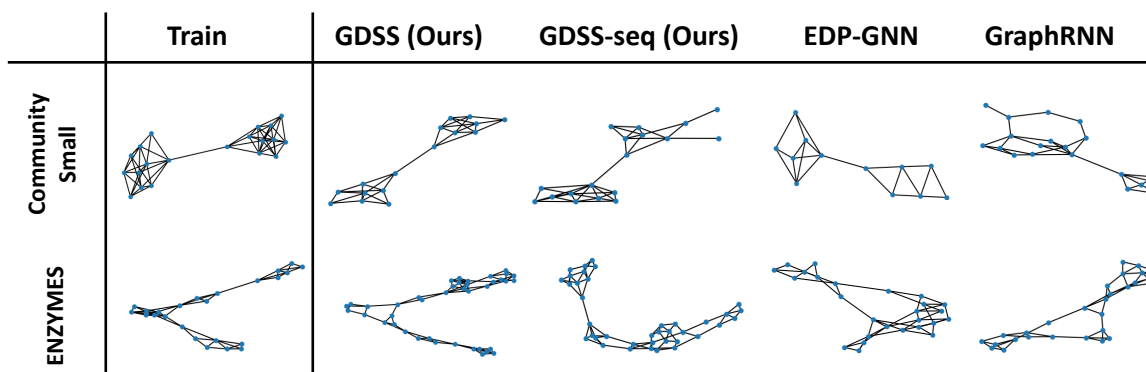


Figure 6: Visualization of generated graphs and the graphs from the training dataset.

E.2. Molecule Generation

We visualize the generated molecules that are maximally similar to certain training molecules in Figure 7. The similarity measure is the Tanimoto similarity based on the Morgan fingerprints, which are obtained by the RDKit (Landrum et al., 2016) library with radius 2 and 1024 bits. As shown in the figure, GDSS is able to generate molecules that are structurally close to the training molecules while other baselines generate molecules that deviate from the training distribution.

	Train	GDSS (Ours)	GDSS-seq (Ours)	GraphAF	MoFlow	GraphDF	EDP-GNN	GraphEBM
QM9		 0.6000	 0.4800	 0.4800	 0.3438	 0.2727	 0.4483	 0.3182
		 0.4242	 0.3125	 0.2750	 0.3514	 0.1667	 0.3529	 0.2857
		 0.5357	 0.3333	 0.2821	 0.3529	 0.1707	 0.4688	 0.3030
ZINC250k		 0.3191	 0.2857	 0.2885	 0.2462	 0.2128	 0.2540	 0.2037
		 0.3519	 0.2941	 0.3111	 0.2593	 0.1633	 0.2571	 0.1730
		 0.3871	 0.3559	 0.3800	 0.2143	 0.1786	 0.3043	 0.1667

Figure 7: Visualization of generated molecules with maximum Tanimoto similarity with the molecule from the dataset. For each generated molecule, we display the similarity value at the bottom. The pairwise Tanimoto similarity is calculated based on the standard Morgan fingerprints with radius 2 and 1024 bits.